Magnetic Resonance in Medicine 52:277–285 (2004)

Imaging Oxygen Consumption in Forepaw Somatosensory Stimulation in Rats Under Isoflurane Anesthesia

Zhaohui M. Liu, Karl F. Schmidt, Kenneth M. Sicard, and Timothy Q. Duong*

The cerebral metabolic rate of oxygen ($CMRO_2$) was dynamically evaluated on a pixel-by-pixel basis in isoflurane-anesthetized and spontaneously breathing rats following graded electrical somatosensory forepaw stimulations (4, 6, and 8mA). In contrast to α-chloralose, which is the most widely used anesthetic in forepaw-stimulation fMRI studies of rats under mechanical ventilation, isoflurane (1.1–1.2%) provided a stable anesthesia level over a prolonged period, without the need to adjust the ventilation volume/rate or sample blood gases. Combined cerebral blood flow signals (CBF) and blood oxygenation level-dependent (BOLD) fMRI signals were simultaneously measured with the use of a multislice continuous arterial spin labeling (CASL) technique (two-coil setup). $CMRO_2$ was calculated using the biophysical BOLD model of Ogawa et al. (Proc Natl Acad Sci USA 1992;89:5951–5955). The stimulus-evoked BOLD percent changes at 4, 6, and 8mA were, respectively, 0.5% ± 0.2%, 1.4% ± 0.3%, and 2.0% ± 0.3% (mean ± SD, $N = 6$). The CBF percent changes were 23% ± 6%, 58% ± 9%, and 87% ± 14%. The $CMRO_2$ percent changes were 14% ± 4%, 24% ± 6%, and 43% ± 11%. BOLD, CBF, and $CMRO_2$ activations were localized to the forepaw somatosensory cortices without evidence of plateau for oxygen consumption, indicative of partial coupling of CBF and $CMRO_2$. This study describes a useful forepaw-stimulation model for fMRI, and demonstrate that $CMRO_2$ changes can be dynamically imaged on a pixel-by-pixel basis in a single setting with high spatiotemporal resolution. Magn Reson Med 52:277–285, 2004. © 2004 Wiley-Liss, Inc.

Key words: fMRI; BOLD; CBF; perfusion; oxidative metabolism; arterial spin labeling; cerebral metabolic rate of oxygen; $CMR_{glucose}$; lactate

Under normal and resting physiological conditions in the brain, almost all (>99%) of the energy required for adenosine triphosphate (ATP) production is supplied by oxidative metabolism, and the cerebral metabolic rate of oxygen ($CMRO_2$) is tightly coupled to the cerebral blood flow (CBF) and the cerebral metabolic rate of glucose ($CMR_{glucose}$) (1). CBF and $CMR_{glucose}$ changes during task-induced increases in neuronal activity have consistently been demonstrated to be similar (~50%) (2,3). However, the magnitude of stimulus-evoked $CMRO_2$ changes remains controversial. Following Fox et al.'s (2) initial study with positron emission tomography (PET), stimulus-evoked $CMRO_2$ changes were reported as negligible (2,4,5), substantial but smaller than the CBF and $CMR_{glucose}$ increases (6–10), or markedly increased by 200–400% (11).

$CMRO_2$ can be measured by various noninvasive techniques, including PET (2,6,12,13), ^{13}C MR spectroscopy (11,14), direct and indirect $H_2^{17}O$ NMR (15), and functional fMRI (fMRI) with biophysical modeling of the blood oxygenation level-dependent (BOLD) signals (7,9,16,17). These techniques all have some unique advantages and disadvantages. PET $CMRO_2$ measurement is based on the Kety-Schmidt method. Multiple physiological parameters must be deconvolved by the application of complex kinetic models to the data sets that are poor in signal-to-noise ratio (SNR). These measurements also take a long time, and multiple measurements cannot be made dynamically or in a single subject. Although ^{13}C spectroscopy and $H_2^{17}O$ NMR techniques can be quantitative, they have relatively poor sensitivity, poor spatiotemporal resolution, and are also highly model-dependent. The $CMRO_2$ technique based on Ogawa et al.'s (18) biophysical BOLD model has the advantage of high spatiotemporal resolution, but it is indirect. The magnitude of the BOLD signal is dependent on CBF and $CMRO_2$ changes: a larger $CMRO_2$ increase for a given ΔCBF yields a smaller the BOLD increase, and vice versa. Thus, relative $CMRO_2$ changes could in principle be derived from BOLD and CBF measurements. Kim and Ugurbil (16) were the first to derive a $CMRO_2$ formalism based on Ogawa et al.'s (18) biophysical BOLD model. They reported a negligible $CMRO_2$ change during visual stimulation in humans (ΔCBF = 43%), consistent with Fox et al.'s (2) initial report. Davis et al. (7) derived a different $CMRO_2$ formalism, also based on Ogawa et al.'s BOLD model, and observed a $\Delta CMRO_2$ of ~16% in the human visual cortex. Hoge et al. (17) extended Davis et al.'s (7) model to investigate graded human visual stimulations, and reported $CMRO_2$ increases of 2–24%.

Most $CMRO_2$ studies have been carried out in humans, and similar studies in animal models are limited. Mandeville et al. (9) derived the $CMRO_2$ formalism based on cerebral blood volume (CBV) instead of CBF. They measured BOLD and CBV sequentially, and performed a region-of-interest (ROI) analysis. Animal models in which $CMRO_2$ can be dynamically measured under controlled conditions could provide valuable insights into the stimulus-evoked changes in cerebral oxygen metabolism, the underlying neural-vascular coupling, and the BOLD signal sources in both normal and diseased states.

In this study, the feasibility of imaging oxygen consumption in association with forepaw stimulation under isoflurane anesthesia using Davis et al.'s (7) $CMRO_2$ formalism was examined. Although almost all previous fMRI studies of rat forepaw stimulation (19–21) used α-chloralose (an

Center for Comparative NeuroImaging, Department of Psychiatry, University of Massachusetts Medical School, Worcester, Massachusetts.

Grant sponsor: Whitaker Foundation; Grant number: RG-02-0005; Grant sponsor: American Heart Association; Grant number: SDG-0430020N; Grant sponsor: National Institute of Health; Grant number: R01-EY014211.

*Correspondence to: Timothy Q. Duong, Ph.D., Center for Comparative NeuroImaging, University of Massachusetts Medical School, 55 Lake Ave. N, Worcester, MA 01655. E-mail: timothy.duong@umassmed.edu

Received 27 October 2003; revised 29 January 2004; accepted 26 February 2004.

DOI 10.1002/mrm.20148
Published online in Wiley InterScience (www.interscience.wiley.com).

analgesic and a mild anesthetic (22)) under mechanically ventilated conditions, a stable level of anesthesia over a relatively long duration is relatively difficult to maintain and is thus less suited for $CMRO_2$ measurements. It was hypothesized that if stable forepaw fMRI activation could be evoked under a gaseous anesthetic, it would be ideal for measuring $CMRO_2$ with high spatiotemporal resolution. Additionally, rats were allowed to breathe spontaneously on their own under isoflurane (as opposed to mechanical ventilation with frequent blood-gas sampling) because it is simpler to set up and the animals can autoregulate their own physiology throughout the experiment without external intervention. More importantly, simultaneous measurements of BOLD and CBF were made using the continuous arterial spin-labeling (CASL) technique with multislice echo-planar imaging (EPI) acquisition. With this animal model and technique, the feasibility of measuring stimulus-evoked $CMRO_2$ changes dynamically and on a pixel-by-pixel basis under graded forepaw stimulation currents was explored.

MATERIALS AND METHODS

Animal Preparation

Six male Sprague Dawley rats (300–375 g) were initially anesthetized with 2% isoflurane. A femoral artery was catheterized with PE-50 tubing, and needle electrodes were inserted under the skin of the forepaws. The rats were secured in an MR-compatible rat stereotaxic headset, and they breathed spontaneously without mechanical ventilation. Anesthesia was reduced to 1.1–1.2% isoflurane, and rectal temperature was monitored and maintained at 37 ± 0.5°C throughout. Heart rate (HR), mean arterial blood pressure (MABP), and respiration rate (RR, derived from the slow modulations on top of the cardiac waveforms) were recorded continuously and analyzed with respect to before and during the "stimulations." Blood gases were typically sampled once during a break between imaging trials.

Hypercapnic Challenge and Forepaw Stimulation

For the hypercapnic challenges, a premixed gas of 10% CO_2, 21% O_2, and balance N_2 was used. A relatively high CO_2 concentration was used because of the smaller hypercapnia-induced fMRI signal changes in anesthetized animals compared to awake animals (23). For forepaw somatosensory stimulation, graded stimulation currents of 4, 6, and 8 mA with 0.3-ms pulse duration at 3 Hz were used. In four of the six rats, a pair of needle electrodes was inserted under the skin of the left forepaw, and another pair was inserted under the skin of the right forepaw. Each forepaw was stimulated separately. In the remaining two rats, electrodes to the two forepaws were connected in series and stimulated simultaneously. For each fMRI trial, data were acquired for 2 min during baseline and 2 min during hypercapnic challenge or forepaw stimulation. Two or three repeated trials were conducted for each condition for each animal. Breaks of ~15 min were given between trials.

MRI Experiments

The MRI experiments were performed on a 4.7-T/40-cm magnet (Oxford, UK), a Biospec Bruker console (Billerica, MA), and a 20-G/cm gradient insert (ID = 12 cm, 120-μs rise time). A surface coil (2.3-cm ID) was used for brain imaging, and a neck coil (20,21) was employed for perfusion labeling. Coil-to-coil electromagnetic interaction was actively decoupled. High-resolution anatomical images were acquired using a fast spin-echo pulse sequence with TR = 2 s, flip angle = 90°, 16 echo trains, effective TE = 104 ms, matrix = 128 × 128, FOV = 2.56 × 2.56 cm^2, eight 1.5-mm slices, and 16 averages.

Combined CBF and BOLD measurements were obtained using the CASL technique (20,21) with a single-shot, gradient-echo, echo-planar imaging (EPI) acquisition. Paired images (one with ASL and one without (control)) were acquired alternately. The MR parameters were as follows: data matrix = 64 × 64, FOV = 2.56 × 2.56 cm^2, eight 1.5-mm slices, TE = 15 ms, TR = 2 s, and flip angle = 90°. For CASL, a 1.78-s square radiofrequency (RF) pulse to the labeling coil was employed in the presence of a 1.0 G/cm gradient along the flow direction, such that the condition of adiabatic inversion was satisfied. The sign of the frequency offset was switched for control images. For each set of the CBF measurements, 31 pairs of images (2 min; the first pair was discarded) were acquired during baseline and 30 pairs (2 min) were acquired during hypercapnic challenge or forepaw stimulation.

Data Analysis

Data analysis employed codes written in Matlab (MathWorks Inc, Natick, MA) and STIMULATE software (24). Repeated CBF measurements of the same condition in each animal were averaged. BOLD images were obtained from nonlabeled images of the CBF measurements. CBF images (S_{CBF}) with intensities in ml/g/min were calculated at each time point (20,21). Cross-correlation analysis was performed on the BOLD, CBF, and $CMRO_2$ data sets to obtain percent-change activation maps.

Calculation of M *and* $CMRO_2$ *Maps*

For the $CMRO_2$ calculation, the model and method described by Davis et al. (7) were used. The notations used herein are based on those of Hoge et al. (17), who rederived Davis et al.'s formalism in detail. $CMRO_2$, CBF, and BOLD signals are related by

$$\frac{\Delta BOLD}{BOLD_0} = M\left(1 - \left(\frac{CMR_{O_2}}{CMR_{O_2}|_0}\right)^{\beta}\left(\frac{CBF}{CBF_0}\right)^{\alpha-\beta}\right), \qquad [1]$$

where M is the proportionality constant, and parameters with subscript zero indicate baseline values. $\alpha = 0.38$ (9,25) and $\beta = 1.5$ (7,26) were used, which were taken to be constants that reflect the effect of blood volume and deoxyhemoglobin concentration to the BOLD signals, respectively. First, pixel-by-pixel M maps from the hypercapnia data were calculated by setting $CMRO_2/CMRO_2|_0$ to one, since brief and mild hypercapnia does not alter $CMRO_2$

(27,28). Using the derived M maps, stimulus-evoked $CMRO_2/CMRO_2|_0$ activation maps were calculated.

To avoid causing bias to a particular current or activation map, percent changes were evaluated using an ROI analysis. ROIs enclosing the primary (~9 pixels) or secondary (~4 pixels) somatosensory cortices were drawn on the average cross-correlation BOLD and CBF activation maps of all currents, with reference to anatomy and brain atlas (the cross-correlation coefficients of the BOLD and CBF activation maps were similar). However, to avoid bias to any particular current or type of activation map, time courses and group-average percent changes were obtained without using masks of the activation maps.

The effects of noise on M and $CMRO_2$ calculation were evaluated. In a manner similar to that used by Davis et al. (7), noise propagation using Monte Carlo simulation was performed with noise characteristics derived from experimental BOLD and CBF data from one representative rat. Data from 1 and 9 pixels (the 1 pixel was selected at the center of the 9-pixel ROI) in the somatosensory cortex were investigated. The input experimental parameters for the simulation were as follows: For hypercapnia, $\Delta BOLD = 3.6\% \pm 0.9\%$, $\Delta CBF = 208\% \pm 55\%$ for 1 pixel; and $\Delta BOLD = 4.7\% \pm 0.4\%$, $\Delta CBF = 189\% \pm 24\%$ for 9 pixels. For 6 mA stimulation, $\Delta BOLD = 0.9\% \pm 0.8\%$, $\Delta CBF = 73\% \pm 45\%$ for 1 pixel; and $\Delta BOLD = 3.3\% \pm 0.3\%$, $\Delta CBF = 163\% \pm 16\%$ for 9 pixels. Additionally, simulations were also performed with the CBF standard deviations (SDs) artificially increased by a factor of 3 for the 9-pixel data.

Coregistration Across Subjects

Raw EPI image data sets (time-course images) from all subjects were manually aligned without spatial interpolation, and averaged with the use of custom-designed software (http://www.quickvol.com). BOLD, CBF, M, and $CMRO_2$ maps were calculated for the coregistered data.

Statistical Analysis

Averaging was performed across repeated measures, the left and right forepaws, the primary and secondary somatosensory cortex, and then across different animals. All CBF and $CMRO_2$ changes were expressed as percentages (instead of ratio of stimulation to baseline). Values in text are mean ± SD, and in the graphs they are mean ± SEM for $N = 6$ rats. Statistical tests were performed by means of a two-tail paired t-test.

RESULTS

Physiological parameters (MABP, HR, and RR) were continuously monitored in all of the animals. Figure 1 shows blood pressure traces before and during forepaw stimulation with 4, 6, and 8 mA from a representative animal, and Table 1 summarizes group-average physiological data before and during forepaw stimulations. At 4 mA, there were no statistically significant transient or sustained changes in these physiological parameters during stimulation relative to baseline. At 6 mA, there were small transient changes in HR ($P = 0.06$) and MABP (< 5 mmHg, $P = 0.01$) immediately following stimulation onset; however, there were no statistically significant changes during the sustained stimulation period ($P > 0.05$). At 8 mA, there was a large transient increase in HR (20 bpm, $P < 0.008$) and MABP (20 mmHg, $P < 0.008$), which remained substantially elevated (20 bpm and 10 mmHg, $P < 0.008$) during stimulation. Additionally, blood gases measured in four of six rats were within normal physiological ranges (pH = 7.45 ± 0.01, $pCO_2 = 37 \pm 1$ mmHg, $pO_2 = 87 \pm 1$ mmHg, O_2 saturation = 91% ± 1%). These values were consistent with previous physiological data obtained in isoflurane-anesthetized rats under spontaneous-breathing conditions (23).

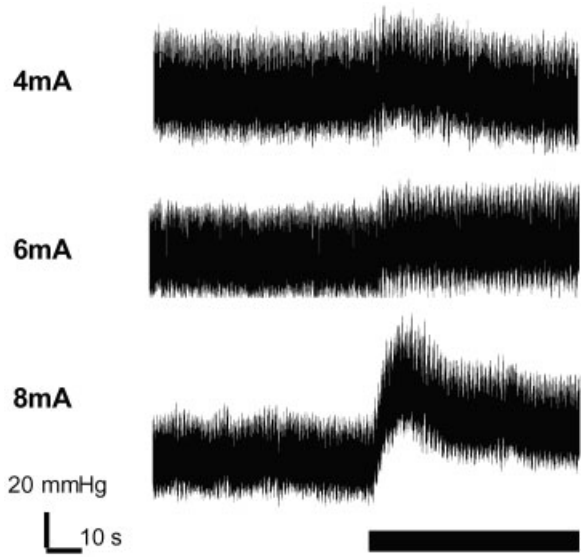

FIG. 1. Representative traces of blood pressure from a rat subjected to graded stimulation currents (4, 6, and 8 mA). The black bars indicate the time period of stimulation (2 min).

Representative anatomical images; CBF images; M maps; and BOLD, CBF, and $CMRO_2$ activation maps from one animal in which two forepaws were simultaneously stimulated are shown in Fig. 2a. M maps were heterogeneous in the brain parenchyma, with larger M values generally localized around the lateral ventricles and the cortical surface, where vascular densities are relatively high. The average M value in the primary somatosensory cortices was 0.05 ± 0.01 (mean ± SD, $N = 6$). The CBF, BOLD, and $CMRO_2$ maps show robust bilateral activation in the primary and secondary somatosensory cortices. The averaged, coregistered BOLD and CBF images, and the BOLD, CBF, and $CMRO_2$ activation maps from all of the animals are shown in Fig. 2b. The averaged, coregistered BOLD and CBF images showed remarkably detailed anatomical structures, without substantial blurring from cross-subject averaging. Unlike the gradient-echo BOLD activation maps, which often showed the highest percent changes in the draining veins or cortical surface vessels, the CBF and $CMRO_2$ activation maps showed large percent changes localized deep in the cortical structures, avoiding surface large-vessel contamination. There were no statistically significant negative-change pixels in the BOLD, CBF, and $CMRO_2$ maps of either single-animal or group-average

Table 1
Physiological Recordings of Respiration Rate (RR), Heart Rate (HR), and Mean Arterial Blood Pressure (MABP) for Six Rats Before and During Forepaw Somatosensory Stimulation Under 4, 6, and 8 mA currents†

Current	RR	HR	MABP
Baseline	61 ± 15	394 ± 35	135 ± 6
4 mA	62 ± 18	386 ± 26 (387 ± 32)	136 ± 6 (136 ± 4)
6 mA	64 ± 15	405 ± 37 (406 ± 39)*	139 ± 11 (141 ± 6)**
8 mA	64 ± 18	415 ± 38** (419 ± 44)***	143 ± 6** (148 ± 8)***

†Mean ± SD, $N = 6$ rats. Values in parentheses are those of the transient (maximum) changes immediately following stimulation onset. The baseline parameters are the average of three stimulation currents; statistical comparisons between baseline and stimulation parameters, however, use pair-wise comparison within each trial. *$P = 0.06$; **$P = 0.01$; ***$P \leq 0.008$ (paired t-test, two tails).

data. Motor activations were sometimes observed with a high current (8 mA), which sometimes caused slight physical movement of the forepaws. In contrast to rat forepaw stimulation studies under α-chloralose (19,21,29), activations in the secondary and subcortical structures (more evident with lower thresholds) were usually detected in the isoflurane-anesthetized animals.

Representative BOLD, CBF, and $CMRO_2$ time courses from ROIs enclosing the primary and secondary somatosensory cortices from one animal are shown in Fig. 3a. Robust dynamic BOLD, CBF, and $CMRO_2$ responses were observed in single animals. Although they were subject to errors resulting from the manner in which the ROIs were drawn, statistical analyses across animals showed that the BOLD, CBF, and $CMRO_2$ percent changes in the primary somatosensory cortices were not statistically different from those of the secondary somatosensory cortices (data not shown), and thus they were grouped together in subsequent analyses. The group-average percent changes are summarized in Fig. 3b. The group-average BOLD percent changes at 4, 6, and 8 mA were 0.5% ± 0.2%, 1.4% ± 0.3%, and 2.0% ± 0.3% (mean ± SD, $N = 6$), respectively. The group-average CBF percent changes at 4, 6, and 8 mA were 23% ± 6%, 58% ± 9%, and 87% ± 14%, respectively. The group-average $CMRO_2$ percent changes at 4, 6, and 8 mA were 14% ± 4%, 24% ± 6%, and 43% ± 11%, respectively. The group-average baseline CBF value was 0.91 ± 0.13 ml/g/min, consistent with previous values reported in rat brain under 1.1–1.2% isoflurane and mechanical ventilation (0.9 ml/g/min) (30), and slightly lower than those reported in 2% isoflurane-anesthetized rats under mechanical ventilation (1.3 ml/g/min) (30) and spontaneous respiration (1.3 ± 3 ml/g/min) (23), as expected.

Correlation plots of BOLD vs. CBF percent changes, and $CMRO_2$ vs. CBF percent changes at 4, 6, and 8 mA for individual animals are shown in Fig. 4. The BOLD vs. CBF, and $CMRO_2$ vs. CBF were linear over the CBF ranges studied. Fractional changes in CBF and $CMRO_2$ coupled linearly with a ratio of 2.2:1. Although data points of different stimulation currents from different animals on the scatterplots overlapped slightly, they were reasonably segregated with 4 mA data points clustered at smaller BOLD, CBF and $CMRO_2$ percent changes, while 8 mA data points clustered at larger percent changes.

Propagation of Errors

The effects of noise propagation on the M and $CMRO_2$ distributions derived from the Monte Carlo simulation are shown in Fig. 5. The resultant M values were 0.050 ± 0.015 for 1 pixel, and 0.068 ± 0.007 for 9 pixels. The resultant $CMRO_2$ values were 30% ± 45% for 1 pixel, and 35% ± 15% for 9 pixels. A marked reduction in the distribution width was observed for 9 pixels. If the SDs of CBF measurements were artificially increased by a factor of 3, the M value was skewed to a lower value and was asymmetrically distributed. However, the $CMRO_2$ distributions were self-correcting and not skewed. Also note that the mean M value for the 1-pixel data was lower than that for the 9-pixel data. However, the maximum-likelihood $CMRO_2$ distributions of the 1- and 9-pixel data were similar.

DISCUSSION

Isoflurane-Anesthetized Forepaw Stimulation Model

A majority of forepaw-stimulation fMRI studies in rats have used α-chloralose and mechanical ventilation (19,21,29). α-chloralose (22) is an analgesic and a mild anesthetic, which minimally suppresses neuronal activity. CBF under α-chloralose (21) is reduced relative to that under awake (23) and isoflurane-anesthetized (23,30) conditions. However, since α-chloralose causes marked respiratory depression, animals generally must be mechanically ventilated, and the ventilation rate and/or volume must be carefully adjusted to maintain physiological parameters within normal ranges based on frequent blood-gas sampling. It is generally more difficult to maintain stable anesthesia over a prolonged period with injectable anesthetics compared to gaseous anesthetics. Therefore, the former is less suited for studies that require multiple repeated measurements over prolonged periods during which $CMRO_2$ could change due to unstable levels of anesthesia.

A previous study (23) and this study demonstrate that the physiology of isoflurane-anesthetized and spontaneously breathing rats can be maintained within normal ranges. Rats reacted to tail-pinching under 0.75% isoflurane but not under 1.1–1.2% isoflurane. Whereas rats under >1.25% isoflurane did not yield significant fMRI responses for the currents explored (data not shown), consistent with previous BOLD and CBF fMRI studies of visual stimulation in cats under 1.0–1.25% isoflurane (31,32). The depth of the anesthesia, as monitored via MABP, HR, and RR, remained relatively stable and constant across ~6–8 hr. Almost all of the repeated measures yielded fMRI responses with stimulation ≥6 mA under

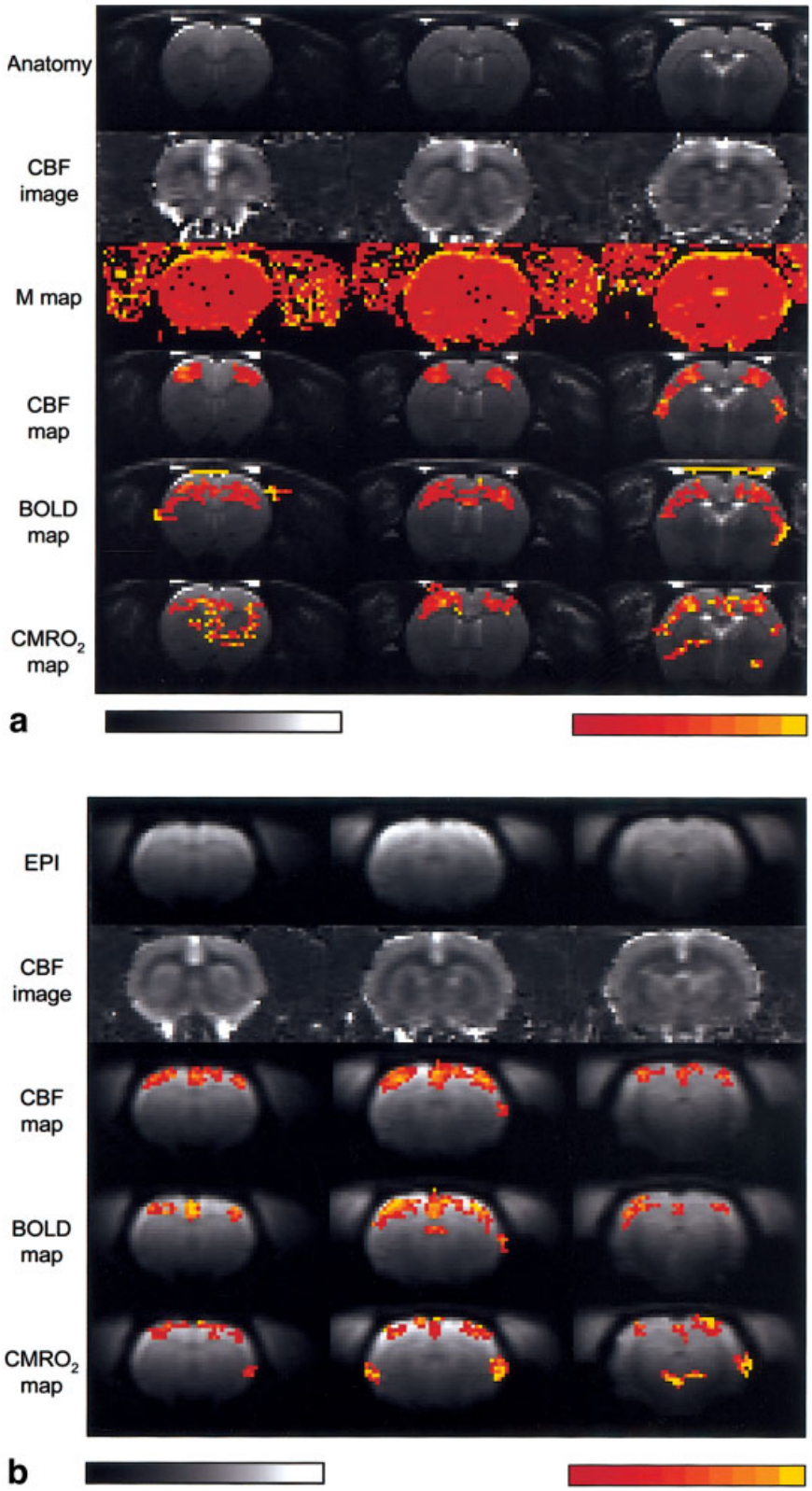

FIG. 2. Representative anatomical images; EPI images; CBF images; and *M*, BOLD, CBF, and $CMRO_2$ maps from (**a**) one rat in which two forepaws simultaneously stimulated, and (**b**) coregistered maps from all animals (6 mA under 1.1–1.2% isoflurane). Maps are overlaid on anatomical images in part **a** and on averaged coregistered EPI images in **b**. Percent thresholds were set for display purposes, and secondary forepaw activations are not visible in some maps. Grayscale bar: CBF values = 0–3 ml/g/min. Color bar: $M \sim$ 1–20%, CBF ~ 80–200%, BOLD ~ 2–10%, $CMRO_2 \sim$ 20–100%.

1.1–1.2% isoflurane. Since this study is the first to use isoflurane for fMRI of forepaw stimulation in rats, multiple graded currents were carefully evaluated while MABP, HR and RR were invasively monitored. The optimal stimulation current, which yielded minimal changes in MABP, HR, and RR, was ~6 mA under 1.1–1.2% isoflurane. Future studies will not require invasive MABP and HR monitoring; therefore, fMRI using this model could be totally noninvasive, which would make longitudinal forepaw fMRI studies possible.

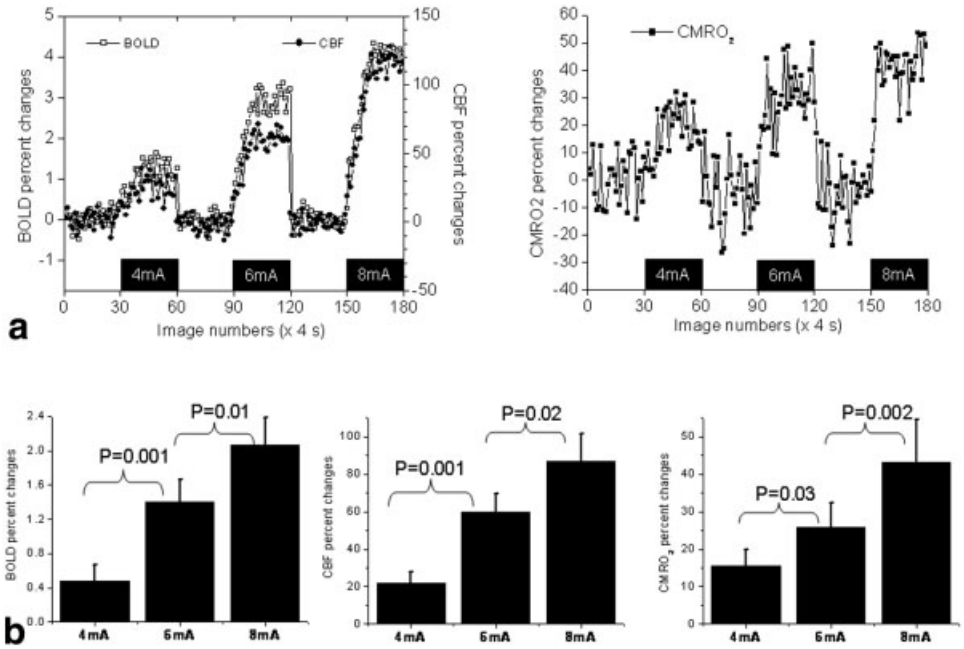

FIG. 3. **a:** Representative BOLD, CBF, and $CMRO_2$ time courses from an ROI enclosing the primary forepaw cortices of one animal (Fig. 2a). The time courses of 4, 6, and 8 mA were concatenated together. The rectangular boxes indicate 4, 6, and 8 mA stimulation currents. **b:** Group average of the BOLD, CBF, and $CMRO_2$ responses to 4, 6, and 8 mA stimulation currents. Error bars are mean ± SEM, $N = 6$ rats.

The use of isoflurane, however, has some disadvantages. Isoflurane suppresses neuronal activity, which reduces fMRI responses. This may explain why higher currents were needed in this study, as compared to the 1.5–2.0 mA commonly used in fMRI studies in rats under α-chloralose anesthesia (19,21,29). Stimulation with 2 mA under 1.1–1.2% isoflurane produced no significant changes in BOLD, CBF, or $CMRO_2$ (data not shown). Another disadvantage is that isoflurane is a potent cerebrovasodilator, (33) which leads to a global increase in CBF. Basal CBF markedly modulates the magnitude and the dynamics of the stimulus-evoked BOLD responses (34,35). High basal CBF could have resulted in a "ceiling effect" in the BOLD and CBF percent changes; however, the current data show that this ceiling effect did not occur under these experimental conditions. Aside from these minor drawbacks, forepaw stimulation under 1.1–1.2% isoflurane anesthesia yields robust fMRI responses and is easy to set up.

Precision and Error Propagation

In addition to the improved anesthetic stability of the isoflurane forepaw-stimulation model over a prolonged period, there was also improvement in the precision of the $CMRO_2$ measurement relative to previous MR-based $CMRO_2$ studies (7,9,10,16,17). First, by using the CASL technique with the two-coil setup, a relatively higher CBF SNR was obtained without employing an exogenous contrast agent. Second, CBF and BOLD were measured simultaneously, which minimized variations from sequential measurements that require the subject to respond identically during separate stimulations. Third, identical imaging parameters (e.g., the EPI readout time) were also used in the CBF and BOLD measurements, which avoid sensitizing the fMRI signals different visible spin populations (signal sources). Finally, the CASL technique with the two-coil setup, in contrast to the flow-sensitive alternating inversion recovery (FAIR) technique (7,9,16,17), has a multislice capability that allows $CMRO_2$ measurements to be made over the entire brain.

In contrast to Davis et al.'s (7) noise propagation simulation, which used an SNR of 100:1 and a FAIR perfusion signal component of 4%, the current noise propagation used the uncertainties from experimental BOLD and CBF measurements from a single representative animal. In

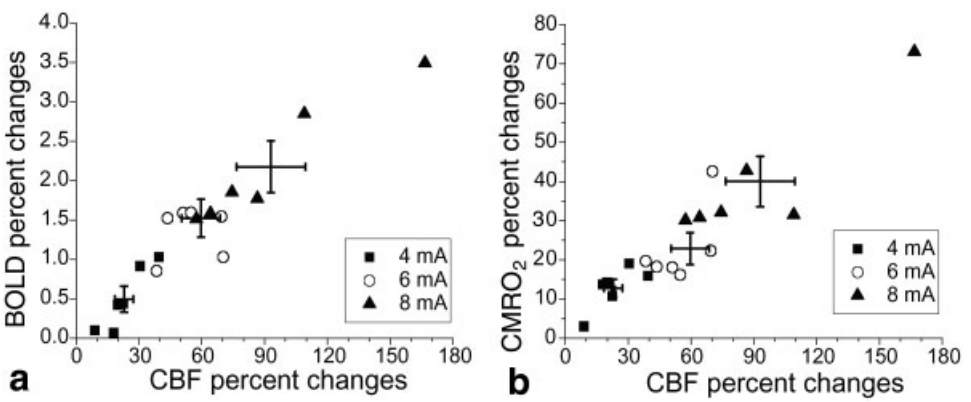

FIG. 4. Correlation plots of (**a**) BOLD vs. CBF, and (**b**) $CMRO_2$ vs. CBF for six rats under 4, 6, and 8 mA currents. The CBF: BOLD and $CMRO_2$:CBF ratios were 40:1 and 2.2:1, respectively, assuming linearity over the parameter ranges. The group-average values for each of the stimulation currents are shown in ± SEM for $N = 6$ rats. Each data point was obtained from one animal.

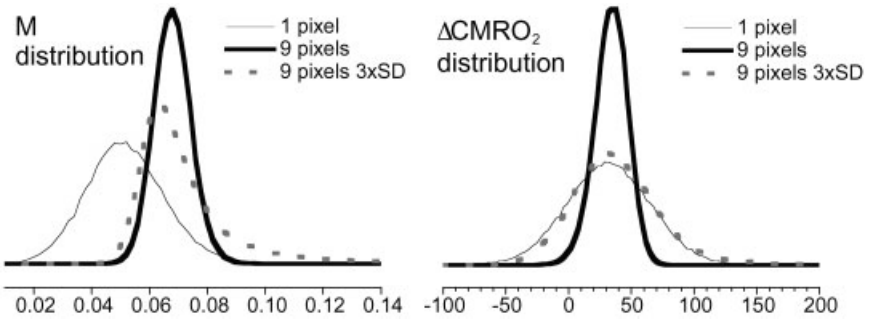

FIG. 5. Noise propagation results from Monte Carlo simulation with means and SDs derived from experimental BOLD and CBF measurements (see Materials and Methods). The *M* distribution is broader and located at a lower value for the 1-pixel data (thin lines) compared to the 9-pixel data (thick lines). Noise added by increasing the CBF SD by a factor of 3 in the 9-pixel data (dotted lines) skews the *M* maximum likelihood. The $CMRO_2$ distributions in all cases show no noise bias.

Davis et al.'s (7) simulation and measurements, the FAIR-based CBF had a relatively poorer SNR compared to BOLD, which was measured separately. Consequently, a skew in the *M* distribution was observed in Davis et al.'s (7) 1-pixel data, resulting from increased variance of the CBF term in the denominator of the *M* equation. In the present study, no skew was observed in the *M* distribution of the 1-pixel data. This is likely because the variances of the CBF and BOLD percent changes were similar, and/or both the CBF and BOLD SNR were higher in the animal study. These conclusions were confirmed by the observation that if the uncertainty in the CBF measurements was artificially increased three times, a small skew became evident in the *M* distribution. Consistent with Davis et al.'s (7) findings, the $CMRO_2$ distribution showed no skew, indicating that poor CBF SNR does not change the expected $CMRO_z$ value, although its uncertainty increases. This is due to the self-correcting nature of the $CMRO_2$ formalism. It is also interesting to note that the *M* maximum likelihood of the single pixel was lower than that of the 9 pixels, but no substantial differences between the 1- and 9-pixel $CMRO_2$ maximum likelihoods were observed. A possible explanation is that this particular single pixel contains a relatively smaller blood volume fraction, but similar $CMRO_2$, relative to the 9-pixel data. Error propagation analyses demonstrate the robustness of the $CMRO_2$ determination, and shed light on the biological significance of the *M* values.

Interpretation of *M* Maps and $CMRO_2$ Maps

The *M* value is specific to a given baseline physiologic state, pulse sequence, and field strength, and is regionally dependent. Differences in *M* values arise from differences in regional CBF, CBV, vascular orientation, and vascular density. BOLD percent changes are dependent on baseline physiology. A larger *M* value yields a larger stimulus-evoked BOLD increase for a given CBF change if other physiologic parameters remain the same. The mean *M* value in the primary somatosensory cortices was 0.05 ± 0.01, which is comparable to that described by Davis et al. (7) (0.079 ± 0.007) and somewhat lower than those reported by Wu et al. (36) (0.16 ± 0.02) and Hoge et al. (17) (0.15 ± 0.06). A longer TE per se in the BOLD measurement yields a larger *M*, and thus only regional differences in *M* maps can be compared (i.e., larger *M* does not affect the stimulus-evoked $CMRO_2$ changes, because the same TE is used in the stimulation experiments).

Cross-laboratory comparisons of stimulus-evoked $CMRO_2$ and CBF changes are summarized in Table 2. In Kim and Ugurbil's formalism (16), a few assumptions (e.g., concerning the baseline venous oxygenation and volume fraction) were made when they derived the $CMRO_2$ changes. The advantage of Davis et al.'s formalism (7) is that all of these parameters and other physiological quantities are lumped into the constant *M*, which can be mea-

Table 2
Cross-Laboratory Comparisons of Stimulus-Evoked $CMRO_2$ and CBF Changes

ΔCBF	$\Delta CMRO_2$	Conditions	Species and brain regions	Reference
50%	5%	PET, Kety-Schmidt method, calibrations on different subjects, $\Delta CMR_{glucose} = 51\%$	Human visual cortex	Fox et al. (2)
43%	0%	Kim's $CMRO_2$ modeling, BOLD and FAIR, global calibration constants, ROI analysis	Human visual cortex	Kim and Ugurbil (16)
45%	16%	Davis's $CMRO_2$ model, BOLD & FAIR, $\Delta CMRO_2$ insensitive to α and β, $\Delta CMRO_2$ maps	Human visual cortex	Davis et al. (7)
$48\%_{max}$	$25\%_{max}$	Davis's model, BOLD and FAIR, graded hypercapnia, graded stimulations, ROI analysis, $\Delta CMRO_2 = 2$–25%	Human visual cortex	Hoge et al. (8,17)
44%	16%	Modified Kim's model of (16), BOLD and FAIR, global calibration constants, ROI analysis	Human visual cortex	Kim et al. (10)
62%	19%	5V stimulation, ventilated under α-chloralose, laser-Doppler CBF, MION CBV, ROI analysis	Rat somato-sensory cortex	Mandeville et al. (19)
23%	14%	4mA	Rat somato-sensory cortex	This study
58%	24%	6mA		
87%	43%	8mA		

1.1% isoflurane, spontaneous breathing rats, simultaneous CBF & BOLD measurements, graded forepaw stimulation, $\Delta CMRO_2$ maps

sured on a pixel-by-pixel basis. Consequently, there are no a priori assumptions regarding the resting blood volume fraction, resting capillary or venous oxygen saturation, blood flow, or metabolic rate of oxygen. Both Kim (16) and Davis (7) measured BOLD and CBF to derive $CMRO_2$. These derivations rely on the Grubb CBV-CBF relation ($CBV = CBF^{\alpha}$), and a whole-brain averaged Grubb's factor ($\alpha = 0.38$) obtained from monkeys (25) was used. Davis et al. (7) showed that $CMRO_2$ is only weakly dependent on the Grubb's factor. Mandeville et al. (19) used CBV instead of CBF measurements to derive $CMRO_2$. By measuring CBV using a blood-pool MION contrast agent, and CBF using a laser Doppler flow technique, Mandeville et al. (19) obtained a Grubb's factor of 0.4 in the rat forepaw somatosensory cortices. Exchanging the CBV with the CBF term in Kim (16), Davis (7), and Mandeville's (9) $CMRO_2$ formalisms assumes that the CBV and CBF dynamics are temporally in synchrony, which is not necessarily valid. However, given the typical temporal resolution of the $CMRO_2$ measurement to date, the CBV-CBF uncoupling in the time domain is unlikely to be a major issue (i.e., steady-state $CMRO_2$ measurements should remain valid) (36). It should be noted that the $CMRO_2$ formalism models the BOLD signal based on total blood volume without distinguishing different (arterioles/capillaries/venules) vascular components. Most stimulus-evoked BOLD signal changes largely reflect oxygenation changes in the venous (not the total) blood volume, which constitute ~71% of total blood volume (37), whereas most stimulus-evoked CBV changes occur in the arterioles, not in the venules/veins (38). Accounting for different vascular compartments in the $CMRO_2$ formalism could potentially yield valuable insights (36). Further improvements and advances in the $CMRO_2$ MRI techniques can be made by validating the assumptions in the $CMRO_2$ formalism, demonstrating the reproducibility of the $CMRO_2$ maps, cross-validating with a microPET $CMRO_2$ technique, experimentally determining α and β on a pixel-by-pixel basis, and measuring $CMRO_2$ at very high temporal resolution (with CBF-CBV uncoupling taken into account).

Stimulus-evoked $CMRO_2$ changes ranged from 14% to 43% for stimulation currents of 4–8 mA. The $CMRO_2$ and CBF relationship could be approximated by a linear function up to a 100% CBF increase. The ratio of the CBF to $CMRO_2$ changes was 2.2:1 for all three stimulation currents, in reasonable agreement with Davis et al. (7) (2.8:1), Hoge et al. (17) (2.0:1), and Kim et al. (10) (2.8:1) in humans, and Mandeville et al. (9) in rats (3.2:1). The magnitude of the $CMRO_2$ changes are consistent with previous studies (6–9,17,39) that showed partial coupling of CBF and oxygen consumption changes, but are inconsistent with those that showed little or no oxygen consumption changes during increased neural activity (2,5,16). The findings of partial coupling support the hypothesis of oxygen diffusion limitation proposed by Buxton et al. (40). However, it remains plausible that the disproportional stimulus-induced increase in CBF does not supply oxygen for oxidative metabolism, but rather serves to remove metabolic by-products, among other functions. Hoge et al. (8) estimated the ATP yield under stimulus-evoked oxidative metabolism in the brain, and concluded that the magnitude of increased $CMRO_2$ was largely sufficient to fuel the increased neuronal activity because of the efficient oxidative pathway. Nevertheless, the disproportionately large stimulus-evoked increase in glucose consumption must be accounted for if the increase is not driven by metabolic demand and/or fueled by inefficient nonoxidative metabolism.

Applications of $CMRO_2$ Imaging

This method of imaging oxygen consumption in a single setting over the entire brain is expected to have many important applications. One application is in fMRI of disease states in which neural-vascular coupling is perturbed, such as stroke. In such cases, the BOLD response may no longer scale with neural activity (at least in a linear fashion) and thus may become difficult to interpret. $CMRO_2$ changes may be a better indicator of the underlying changes in brain functions associated with ischemic brain injury. This technique could also offer a means of resolving disease-related perturbations in hemodynamic coupling and oxygen metabolism. Another application of $CMRO_2$ imaging is in pharmacological fMRI. Following drug administration, the baseline physiologic states of the brain are likely to be different regionally or globally due to drug-induced changes in respiration rates, blood pressure and/or volume, and drug-induced vasodilation or vasoconstriction. These alterations, which are independent of the drug-induced changes in neural activity, could markedly affect the fMRI signals. $CMRO_2$ imaging could be used to differentiate nonneural from neural drug effects in pharmacological fMRI. Furthermore, $CMRO_2$ imaging at higher temporal resolution could potentially shed light on the signal source of the initial negative BOLD (dip), which may be a more spatially specific mapping signal (31,32).

CONCLUSIONS

This study has established an isoflurane-anesthetized and spontaneous-breathing rat model for fMRI studies of forepaw stimulation, and demonstrated that stimulus-evoked $CMRO_2$ maps could be dynamically acquired in a single setting on a pixel-by-pixel basis. BOLD, CBF, and $CMRO_2$ changes showed activations localized to the forepaw primary and secondary somatosensory cortices, and scaled with stimulation strengths. The magnitude of the $CMRO_2$ changes is consistent with partial coupling of CBF and oxygen consumption during increased neural activity. $CMRO_2$ imaging has the potential to provide valuable insights into the underlying neural-vascular coupling and the BOLD signal sources. This model and technique are also expected to have important applications in fMRI of disease states, as well as in pharmacological fMRI for conditions in which the baseline physiology is dynamically perturbed.

REFERENCES

1. Siesjo B. Brain energy metabolism. New York: Wiley; 1978.
2. Fox PT, Raichle ME, Mintun MA, Dence C. Nonoxidative glucose consumption during focal physiologic neural activity. Science 1988; 241:462–464.

3. Raichle ME. Circulatory and metabolic correlates of brain function in normal humans. In: Plum F, editors. Handbook of physiology—the nervous system. Vol. V. Higher functions of the brain. Bethesda: American Physiological Society; 1987. p 643–674.
4. Madsen PL, Linde R, Hasselbalch SG, Paulson OB, Lassen NA. Activation-induced resetting of cerebral oxygen and glucose uptake in the rat. J Cereb Blood Flow Metab 1998;18:742–748.
5. Madsen PL, Hasselbalch SG, Hagemann LP, Olsen KS, Bulow J, Holm S, Wildschiodtz G, Paulson OB, Lassen NA. Persistent resetting of the cerebral oxygen/glucose uptake ratio by brain activation: evidence obtained with the Kety-Schmidt technique. J Cereb Blood Flow Metab 1995;15:485–491.
6. Roland PE, Ericksson L, Stone-Elander S, Widen L. Does mental activity change the oxidative metabolism of the brain? J Neurosci 1987;7: 2373–2389.
7. Davis TL, Kwong KK, Weisskoff RM, Rosen BR. Calibrated functional MRI: mapping the dynamics of oxidative metabolism. Proc Natl Acad Sci USA 1998;95:1834–1839.
8. Hoge RD, Atkinson J, Gill B, Crelier GR, Marrett S, Pike GB. Linear coupling between cerebral blood flow and oxygen consumption in activated human cortex. Proc Natl Acad Sci USA 1999;96:9403–9408.
9. Mandeville JB, Marota JJ, Ayata C, Moskowitz MA, Weisskoff RM, Rosen BR. MRI measurement of the temporal evolution of relative CMRO2 during rat forepaw stimulation. Magn Reson Med 1999;42: 944–951.
10. Kim S-G, Rostrup E, Larsson HBW, Ogawa S, Paulson OB. Simultaneous measurements of CBF and CMRO2 changes by fMRI: significant increase of oxygen consumption rate during visual stimulation. Magn Reson Med 1999;41:1152–1161.
11. Hyder F, Chase JR, Behar KL, Mason GF, Siddeek M, Rothman DL, Shulman RG. Increased tricarboxylic acid cycle flux in rat brain during forepaw stimulation detected with 1H[13C]NMR. Proc Natl Acad Sci USA 1996;94:7612–7617.
12. Fox PT, Raichle ME. Focal physiological uncoupling of cerebral blood flow and oxidative metabolism during somatosensory stimulation in human subjects. Proc Natl Acad Sci USA 1986;83:1140–1144.
13. Marrett S, Fujita H, Meyer E, Ribeiro L, Evans AC, Huwabara H, Giedde A. Stimulus specific increase of oxidative metabolism in human visual cortex. In: Uemura K, Lassen NA, Jones T, Kanno I, editors. Quantification of brain function, tracer kinetics and image analysis in brain PET. New York: Excerpta Medica; 1993. p 217–228.
14. Hyder F, Rothman DL, Mason GF, Rangarajan A, Behar KL, Shulman RG. Oxidative glucose metabolism in rat brain during single forepaw stimulation: a spatially localized 1H[13C] nuclear magnetic resonance study. J Cereb Blood Flow Metab 1997;17:1040–1047.
15. Ronen I, Merkle H, Ugurbil K, Navon G. Imaging of H2(17)O distribution in the brain of a live rat by using proton-detected 17O MRI. Proc Natl Acad Sci USA 1998;95:12934–12939.
16. Kim S-G, Ugurbil K. Comparison of blood oxygenation and cerebral blood flow effects in fMRI: estimation of relative oxygen consumption change. Magn Reson Med 1997;38:59–65.
17. Hoge RD, Atkinson J, Gill B, Crelier GR, Marrett S, Pike GB. Investigation of BOLD signal dependence on cerebral blood flow and oxygen consumption: the deoxyhemoglobin dilution model. Magn Reson Med 1999;42:849–863.
18. Ogawa S, Tank DW, Menon R, Ellermann JM, Kim S-G, Merkle H, Ugurbil K. Intrinsic signal changes accompanying sensory stimulation: functional brain mapping with magnetic resonance imaging. Proc Natl Acad Sci USA 1992;89:5951–5955.
19. Mandeville JB, Marota JJ, Kosofsky BE, Keltner JR, Weissleder R, Rosen BR, Weisskoff RM. Dynamic functional imaging of relative cerebral blood volume during rat forepaw stimulation. Magn Reson Med 1998; 39:615–624.
20. Silva AC, Lee S-P, Yang C, Iadecola C, Kim S-G. Simultaneous BOLD and perfusion functional MRI during forepaw stimulation in rats. J Cereb Blood Flow Metab 1999;19:871–879.
21. Duong TQ, Silva AC, Lee S-P, Kim S-G. Functional MRI of calcium-dependent synaptic activity: cross correlation with CBF and BOLD measurements. Magn Reson Med 2000;43:383–392.
22. Nakao Y, Itoh Y, Kuang T-Y, Cook M, Jehle J, Sokoloff L. Effects of anesthesia on functional activation of cerebral blood flow and metabolism. Proc Natl Acad Sci USA 2001;98:7593–7598.
23. Sicard K, Shen Q, Brevard M, Sullivan R, Ferris CF, King JA, Duong TQ. Regional cerebral blood flow and BOLD response in conscious and anesthetized rats under basal and hypercapnic conditions: implications for fMRI studies. J Cereb Blood Flow Metab 2003;23:472–481.
24. Strupp JP. Stimulate: a GUI based fMRI analysis software package. NeuroImage 1996;3:S607.
25. Grubb RL, Raichle ME, Eichling JO, Ter-Pogossian MM. The effects of changes in PaCO2 on cerebral blood volume, blood flow, and vascular mean transit time. Stroke 1974;5:630–639.
26. Boxerman JL, Hamberg LM, Rosen BR, Weisskoff RM. MR contrast due to intravascular magnetic susceptibility perturbations. Magn Reson Med 1995;34:555–566.
27. Kety SS, Schmidt CF. The effects of altered arterial tensions of carbon dioxide and oxygen on cerebral blood flow and cerebral oxygen consumption of normal young men. J Clin Invest 1948;27:484–491.
28. Novack P, Shenkin H, Bortin L, Goluboff B, Soffe AM. The effects of carbon dioxide inhalation upon the cerebral blood flow and cerebral oxygen consumption in vascular disease. J Clin Invest 1953;32:696–702.
29. Silva AC, Lee S-P, Iadecola C, Kim S-G. Early temporal characteristics of CBF and deoxyhemoglobin changes during somatosensory stimulation. J Cereb Blood Flow Metab 2000;20:201–206.
30. Duong TQ, Iadacola C, Kim S-G. Effect of hyperoxia, hypercapnia and hypoxia on cerebral interstitial oxygen tension and cerebral blood flow in the rat brain: an 19F/1H study. Magn Reson Med 2001;45:61–70.
31. Duong TQ, Kim D-S, Ugurbil K, Kim S-G. Spatio-temporal dynamics of the BOLD fMRI signals in cat visual cortex: toward mapping columnar structures using the early negative response. Magn Reson Med 2000; 44:231–242.
32. Duong TQ, Kim D-S, Ugurbil K, Kim S-G. Localized blood flow response at sub-millimeter columnar resolution. Proc Natl Acad Sci USA 2001;98:10904–10909.
33. Matta BF, Heath KJ, Tipping K, Summors AC. Direct cerebral vasodilatory effects of sevoflurane and isoflurane. Anesthesiology 1999;91: 677–680.
34. Kemna LJ, Posse S. Effect of respiratory CO2 changes on the temporal dynamics of the hemodynamic response in functional MR imaging. NeuroImage 2001;14:642–649.
35. Cohen ER, Ugurbil K, Kim S-G. Effect of basal conditions on the magnitude and dynamics of the blood oxygenation level-dependent fMRI response. J Cereb Blood Flow Metab 2002;22:1042–1053.
36. Wu G, Luo F, Li Z, Zhao X, Li SJ. Transient relationships among BOLD, CBV, and CBF changes in rat brain as detected by functional MRI. Magn Reson Med 2002;48:987–993.
37. Duong TQ, Kim S-G. In vivo MR measurements of regional arterial and venous blood volume fractions in intact rat brain. Magn Reson Med 2000;43:392–402.
38. Lee S-P, Duong TQ, Yang G, Iadecola C, Kim S-G. Relative changes of cerebral arterial and venous blood volumes during hypercapnia: implications on BOLD fMRI. Magn Reson Med 2001;45:791–800.
39. Katayama Y, Tsubokawa T, Hirayama T, Kido G, Tsukiyama T, Iio M. Response of regional cerebral blood flow and oxygen metabolism to thalamic stimulation in humans as revealed by positron emission tomography. J Cereb Blood Flow Metab 1986;6:637–641.
40. Buxton RB, Frank LR. A model for the coupling between cerebral blood flow and oxygen metabolism during neural stimulation. J Cereb Blood Flow Metab 1997;17:64–72.